J Solid State Electrochem (2016) 20:225–234
DOI 10.1007/s10008-015-3027-0

ORIGINAL PAPER

Oxygen non-stoichiometry and mixed conductivity of $La_{0.5}Sr_{0.5}Fe_{1-x}Mn_xO_{3-\delta}$

A. A. Markov[1] · K. Yu. Chesnokov[1] · M. V. Patrakeev[1] · I. A. Leonidov[1] · A. V. Chukin[2] · O. N. Leonidova[1] · V. L. Kozhevnikov[1]

Received: 24 July 2015 / Revised: 16 August 2015 / Accepted: 18 August 2015 / Published online: 29 August 2015

Abstract Oxygen non-stoichiometry, thermal expansion, and high-temperature transport properties of perovskite-type $La_{0.5}Sr_{0.5}Fe_{1-x}Mn_xO_{3-\delta}$, where x=0, 0.10, 0.17, 0.25, and 0.33 have been studied in the oxygen partial pressure range 10^{-19} to 0.5 atm. The major trends observed under oxidizing and reducing conditions were found to exhibit substantial differences due to changes in the manganese oxidation state. The high p_{O_2} range is characterized with replacement of Fe^{4+} by Mn^{4+} cations, which results in the decreasing concentration of mobile *p*-type electronic carriers, oxygen non-stoichiometry, and thermal expansion. The oxygen pressure decrease below 10^{-5} atm is accompanied with gradual reduction of manganese to Mn^{3+}/Mn^{4+} mixed oxidation state, followed by larger variations in the non-stoichiometry, electrical conductivity, and thermal expansion. The observed increase in the oxygen ion conductivity with manganese content can be explained as a consequence of strong Mn preference for fivefold oxygen coordination in the oxygen-deficient perovskite lattice, which promotes the formation of oxygen vacancies available for anion diffusion. The calculated oxygen permeation fluxes through $La_{0.5}Sr_{0.5}Fe_{0.67}Mn_{0.33}O_{3-\delta}$ membranes at 950 °C become higher compared with $La_{0.5}Sr_{0.5}FeO_{3-\delta}$, which may be advantageous for application in the integrated processes of oxygen separation, partial hydrocarbon oxidation, and hydrogen production.

✉ M. V. Patrakeev
patrakeev@ihim.uran.ru

[1] Institute of Solid State Chemistry, UB RAS, 91 Pervomaiskaya Str, 620990 Yekaterinburg, Russia

[2] Ural Federal University, 19 Mira Str, 620002 Yekaterinburg, Russia

Keywords Manganese substituted lanthanum-strontium ferrite · Perovskite · Mixed conductor · Thermal expansion · Oxygen membrane

Introduction

The partial oxidation of methane (POM) in catalytic membrane reactors has been considered in recent years as one of the most promising applications for oxides with mixed, ion and electron, conductivity [1–5]. This technology is envisioned as a mode of operation where oxygen separation from air and partial oxidation of methane to synthesis gas is integrated into a single-step process, thereby suggesting better ecology and considerable economic benefits of the processing [6]. Perovskite-like cobaltites have been attracting much attention for the development of membrane materials since discovery of their high oxygen permeability [7, 8]. However, these oxides exhibit excessively large dimensional changes [9] and poor stability at heating in reducing conditions. For instance, reduction of lanthanum cobaltite at 1000 °C takes place readily at fairly high partial pressure of oxygen, p_{O_2} = 10^{-7} atm [10]. Hence, cobalt-based perovskite-like compounds may be utilized only in relatively oxidizing atmospheres, e.g., for oxygen separation from air, while severe reducing conditions of the POM process require more robust cobalt-free materials [11–15]. The ferrous perovskite-like oxides can possibly present a favorable alternative. It is seen, e.g., from work [10] where decomposition of lanthanum ferrite at 1000 °C is reported at 10^{-17} atm. On the other hand, the research into high-temperature transport properties of solid solutions $La_{1-x}Sr_xFeO_{3-\delta}$ gives evidence to large ion conductivity values in the ferrites that may achieve 0.27–0.46 S/cm at x=0.5 and 850–950 °C [16]. Moreover, the ferrite ceramic

membranes demonstrate rather stable properties for more than 7000 h in long-term tests of bench scale POM reactors [17]. Therefore, the preliminary data show that the perovskite-like ferrites, such as $La_{0.5}Sr_{0.5}FeO_{3-\delta}$, can be used as a good matrix for the development of novel POM membrane materials with improved functional characteristics such as oxygen permeability and dimensional stability at heating.

Doping is often employed in order to modify functional properties of perovskite-like oxides. For instance, partial substitution of iron in $SrFeO_{3-\delta}$ with cations having an invariable oxidation state, such as Sc^{3+}, Al^{3+}, or W^{6+}, is favorable for stabilization of the cubic crystalline structure in a wide temperature range. However, the conductivity appears to become noticeably smaller in the doped derivatives than in the parent ferrite [18–20]. More promising seems to be the using of lighter 3d neighbors of iron such as chromium and manganese. These metals form structurally similar solid solutions, $La_{1-x}Sr_xCrO_{3-\delta}$ and $La_{1-x}Sr_xMnO_{3-\delta}$, which are known as good electron conductors. In addition, chromites and manganites exhibit better stability at wide variations of oxygen pressure and temperature than similar perovskite-like cobaltites [21]. At choosing the most appropriate modifier for $La_{1-x}Sr_xFeO_{3-\delta}$, one has to keep in mind also that chromium doping is known to strongly suppress oxygen transport [22]. This phenomenon seems to be a result of the strong preference of chromium cations in perovskite-related structures to rigid octahedral oxygen coordination. In contrast, substitution of iron with manganese may be quite beneficial for oxygen transport because in addition to sixfold environment manganese cations can often adopt fivefold oxygen coordination. For instance, according to works [23, 24], manganese cations in $CaMnO_{2.5}$ and $SrMnO_{2.5}$ maintain fivefold, square pyramidal oxygen coordination. One can expect, therefore, that partial substitution of iron with manganese may help to enhance mobility of oxygen. The other positive effect of manganese doping may be related with decreased thermal expansion of the doped derivatives $La_{0.5}Sr_{0.5}Fe_{1-x}Mn_xO_{3-\delta}$ as it occurs with $Ca_2Fe_{2-x}Mn_xO_{3-\delta}$ [25].

The oxygen transport in perovskite-like ferrite-manganites of lanthanum-strontium has been a subject of research interest already. Thus, authors [26] examined oxygen permeability of $La_{1-x}Sr_xFe_{0.5}Mn_{0.5}O_{3-\delta}$ and $Sr_{1-w}Fe_yMn_{1-y}O_{3-\delta}$ ceramic membranes under He/air gradient. Oxygen chemical diffusion coefficients in $La_{0.5}Sr_{0.5}Fe_{0.7}Mn_{0.3}O_{3-\delta}$ and $La_{0.6}Sr_{0.4}Fe_{0.8}Mn_{0.2}O_{3-\delta}$ were obtained by TG relaxation technique in work [27]. Authors [26, 27] studied solid solutions $La_{1-x}Sr_xFe_{1-y}Mn_yO_{3-\delta}$ at different x's and y's. Note, however, that compositions $La_{0.5}Sr_{0.5}Fe_{0.5}Mn_{0.5}O_{3-\delta}$ [26] and $La_{0.5}Sr_{0.5}Fe_{0.7}Mn_{0.3}O_{3-\delta}$ [27] were considered only in the series $La_{0.5}Sr_{0.5}Fe_{1-x}Mn_xO_{3-\delta}$. It is important to notice also that oxygen permeation and chemical diffusion studies into mixed ferrites-manganites were carried out but at small gradients of oxygen partial pressure, (He or N_2)/air. In such oxidizing conditions, manganese in $La_{1-x}Sr_xFe_{1-y}Mn_yO_{3-\delta}$ is known to maintain 4+ oxidation state [26, 27], which may hinder oxygen vacancy formation and oxygen ion transport. At the same time, the amount of oxygen vacancies in $La_{1-x}Sr_xMnO_{3-\delta}$ tends to increase with the pressure decrease below 10^{-5} atm where it may be as large as $\delta=x/2$ [28]. Clearly, such a large number of the vacancies are expected to ensure respectively large oxygen ion conductivity. However, the available literature data do not allow one to systematically track variations of oxygen transport with manganese content and oxygen pressure, and evaluate oxygen separating efficiency of $La_{0.5}Sr_{0.5}Fe_{1-x}Mn_xO_{3-\delta}$ at large oxygen pressure gradients typical for POM process.

The present work is aimed at studying the effects of iron substitution by manganese in $La_{0.5}Sr_{0.5}FeO_{3-\delta}$ with the emphases on transport properties and dimensional changes induced by variations of temperature and oxygen partial pressure. The experimental data are employed in order to consider the potential of the synthesized materials for the using as ceramic oxygen separating membranes.

Experimental

The samples $La_{0.5}Sr_{0.5}Fe_{1-x}Mn_xO_{3-\delta}$, where x=0, 0.10, 0.17, 0.25, and 0.33, were prepared by solid-state synthesis. The starting high-purity reagents La_2O_3, Fe_2O_3, MnO_2, and $SrCO_3$ were annealed at appropriate temperatures in order to remove adsorbates, weighted in necessary proportions, mixed thoroughly in alcohol media with a mortar and pestle, dried out, and calcined at 1000, 1100, and 1200 °C for 10 h with intermediate regrinding. The resulting powders were pressed uniaxially into discs and sintered for 10 h (Table 1). The apparent density of the obtained ceramics was 93–95 %. Rectangular bars of 2×2×12 and 2×2×8 mm^3 were cut from the sintered discs for electrical and dilatometric measurements, respectively. The samples were partly pulverized for X-ray powder diffraction (XRD), thermogravimetric measurements, and coulometric titration.

Table 1 Sintering temperatures and rhombohedral unit cell parameters of $La_{0.5}Sr_{0.5}Fe_{1-x}Mn_xO_{3-\delta}$

x	Sintering temperature, °C	a, Å	c, Å	a_p, Å	Ref.
0		5.51107	13.41578		[33]
0	1300	5.506 (4)	13.412 (4)	3.886 (1)	
0.10	1350	5.506 (5)	13.414 (7)	3.886 (6)	
0.17	1400	5.503 (3)	13.406 (6)	3.884 (3)	
0.25	1450	5.497 (4)	13.396 (3)	3.880 (6)	
0.30		5.495 (1)	13.379 (1)		[27]
0.33	1500	5.491 (6)	13.376 (8)	3.875 (9)	

The XRD data were collected with the help of an XPert Pro diffractometer (Cu K_α radiation) at room temperature. The obtained diffraction patterns were employed for determination of crystal lattice parameters with the using of a FullProf calculation package [29].

The weight variations due to oxygen losses on heating in air were measured by a Setaram Setsys Evolution-1750 thermoanalyzer at heating rate 5 °C/min. Thermal expansion of the ceramic samples in air and in a reducing gas mixture, 5 % CO–5 % CO_2–Ar, was measured with the using of a Linseis L75 dilatometer. The heating rate was 5 °C/min. The gas mixture flow was maintained at 20 ml/min.

The isothermal variations of oxygen content $(3-\delta)$ in $La_{0.5}Sr_{0.5}Fe_{1-x}Mn_xO_{3-\delta}$ at changes of oxygen partial pressure over samples were measured by means of a coulometric titration technique. This method is based on oxygen pumping and sensing properties of solid-state oxygen electrolytes, and it enables precise measurements of oxygen equilibrium pressure (activity) over a studied sample in the enclosed volume of the titration cell [30].

The simultaneous measurements of conductivity (σ) and thermopower (S) in ceramic bar-like specimens $La_{0.5}Sr_{0.5}Fe_{1-x}Mn_xO_{3-\delta}$ were carried out also in a cell outfitted with solid-state oxygen electrochemical sensor and pump. One specimen, equipped with butt electrodes and thermocouples, was used for measurements of thermopower. The temperature gradient in the furnace along the sample was about 20 K/cm. Another sample was used in four-probe d.c. conductivity measurements. Current leads of platinum wire (0.3 mm) were tightly wound to the sample at 10-mm spacing, while the spacing between the potential probes was about 8 mm. The bar for conductivity measurements was placed perpendicular to the similar specimen for thermopower measurements, which enabled maintenance of zero temperature gradient along the bar. The measurements were carried out in isothermal runs at pressure decrease and halted upon achievement of the desirable low-pressure limit. Then, the oxygen pressure was increased to the starting upper limit where measurements were repeated in order to confirm reversibility of the experiment; thereupon, temperature was changed thus enabling the next measuring cycle. After collecting the data for equilibrium conductivity, additional measurements were carried out down to extremely low pressures of oxygen in order to determine stability limits of the materials under reducing conditions. The incipient decomposition of the material was signaled by a sharp decline of conductivity.

The coulometric titration, conductivity, and thermopower measurements were performed at oxygen partial pressure variations between 10^{-19} and 0.5 atm in the temperature range 800–950 °C. The equilibration criteria were accepted continuous slow changes $d(\log(p_{O_2}/\text{atm}))/dt < 0.001\ \text{min}^{-1}$, $d(\log(\sigma/\text{S}\cdot\text{cm}^{-1}))/dt < 0.0001\ \text{min}^{-1}$, and $d(S/\mu\text{V}\cdot\text{K}^{-1})/dt < 0.001\ \text{min}^{-1}$ for oxygen pressure in the coulometric titration cell, and for conductivity and thermopower values, respectively. The relaxation time varied from 20 min to several hours depending on temperature and partial pressure of oxygen. The electrical parameters were measured with a high-precision Solartron 7081 voltmeter. Additional experimental details can be found elsewhere [31, 32].

Results and discussion

The X-ray powder diffraction patterns of $La_{0.5}Sr_{0.5}Fe_{1-x}Mn_xO_{3-\delta}$ (where x=0, 0.10, 0.17, 0.25, and 0.33) evidence formation of single phases with perovskite-like rhombohedral structure (S.G. $R\bar{3}c$) at room temperature (Fig. 1). The unit cell parameters a and c, and the normalized pseudocubic cell parameter a_p for the synthesized samples are shown in Table 1. The structural parameters obtained in this work for x=0 and x=0.33 are in a good correspondence with the earlier data [27, 33]. One can see also from Table 1 that the increase in manganese content is accompanied with the decrease of the unit cell parameters. This change is consistent with replacement of iron, Fe^{4+} (R_{CN6}=0.585 Å) for smaller manganese cations, Mn^{4+} (R_{CN6}=0.530 Å) [34].

The results of thermogravimetric measurements in air are shown in Fig. 2 where it is seen that the relative weight change due to oxygen loss at heating tends to decrease with the increase of manganese content. This behavior is in accord with the data in work [26] where 4+ charged state of the manganese dopant is shown to preferably exist in the ferrites in air conditions. It is

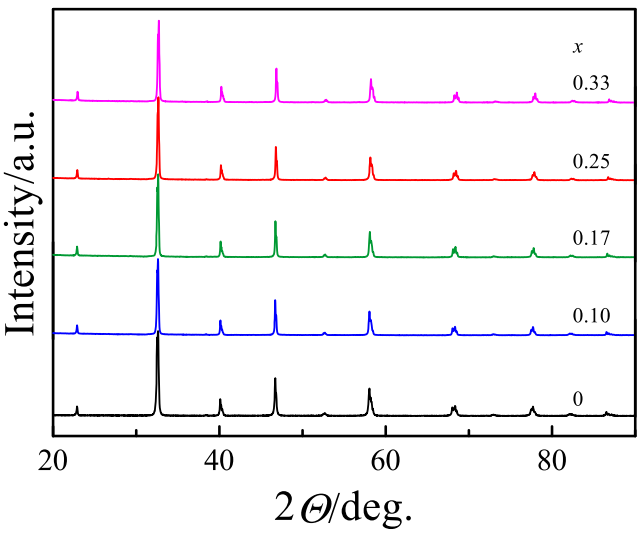

Fig. 1 X-ray diffraction patterns of $La_{0.5}Sr_{0.5}Fe_{1-x}Mn_xO_{3-\delta}$ at room temperature

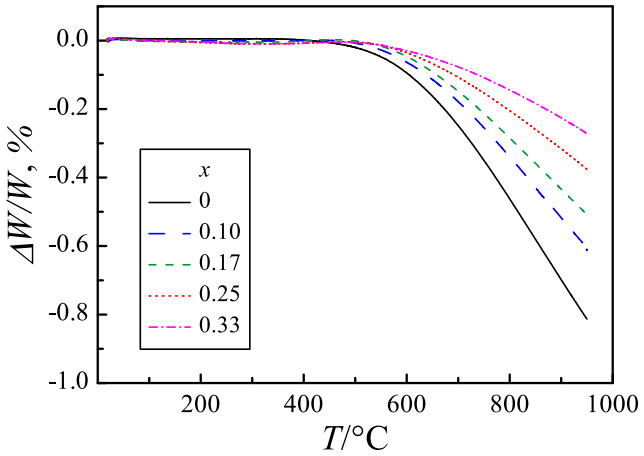

Fig. 2 The relative weight changes observed on heating of $La_{0.5}Sr_{0.5}Fe_{1-x}Mn_xO_{3-\delta}$ in air. Heating rate is 5 °C/min

well documented in the literature that large variations of δ are often accompanied with respectively large dimensional changes of the crystalline lattice. Therefore, it is quite naturally to observe a decrease in the linear expansion of $La_{0.5}Sr_{0.5}Fe_{1-x}Mn_xO_{3-\delta}$ ceramics at heating in air with the increase of manganese content (Fig. 3a, Table 2). Hence, manganese substitution for iron appears to be a promising approach for improvement of thermo-mechanical characteristics of $La_{0.5}Sr_{0.5}Fe_{1-x}Mn_xO_{3-\delta}$ membrane materials. However, one has to keep in mind that ceramic membranes for partial oxidation of methane are supposed to operate under large gradients of oxygen partial pressure. Therefore, the influence of reducing atmospheres upon materials' behavior and characteristics must be considered in order to be able to assess their applicability for POM process.

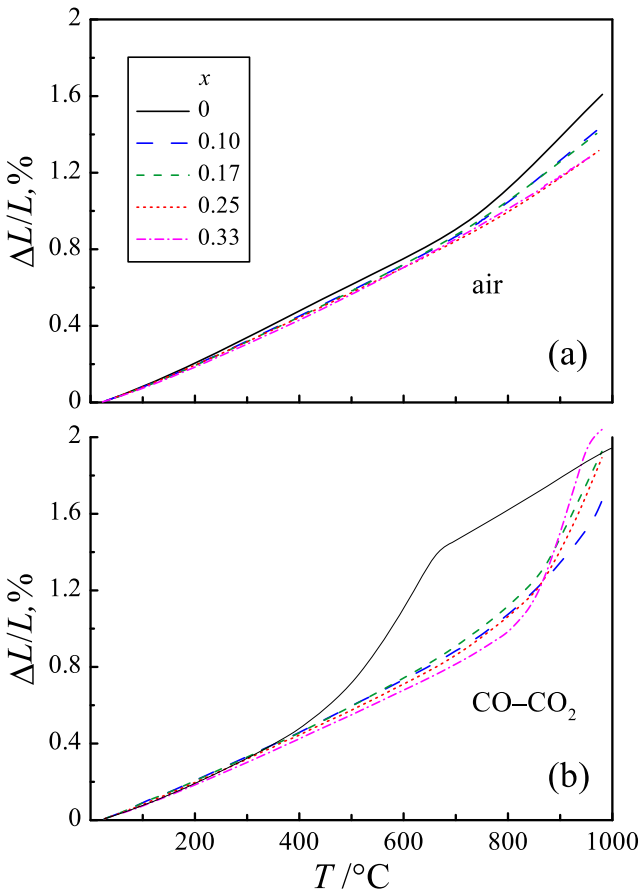

Fig. 3 Relative elongation of $La_{0.5}Sr_{0.5}Fe_{1-x}Mn_xO_{3-\delta}$ ceramics on heating in air (**a**) and in reductive gas mixture 5 % CO–5 % CO_2–Ar. Heating rate is 5 °C/min. The flow rate of gas mixture is 20 ml/min

The coulometric titration data for $La_{0.5}Sr_{0.5}Fe_{1-x}Mn_xO_{3-\delta}$ at 950 °C and different x's are shown in Fig. 4. The oxygen content $(3-\delta)=2.75$ in $La_{0.5}Sr_{0.5}FeO_{3-\delta}$ at 950 °C and $p_{O_2}=2.3\times10^{-10}$ atm was found from the inflection point on the respective isotherm as shown by the maximum of the derivative $(-\partial\delta/\partial p_{O_2})$. This singular oxygen content occurs when average oxidation degree 3+ of iron cations is attained in the oxide with $x=0$ [35]. Further comparison with the data from thermogravimetric measurements makes it possible to deduce $\delta=0$ in $La_{0.5}Sr_{0.5}FeO_{3-\delta}$ when the specimen is equilibrated in air at 950 °C and slowly cooled down to room temperature. Accordingly, the average oxidation degree 3.5+ of iron in such a sample is smaller than the oxidation degree 4+ of manganese. Hence, substitution of manganese for iron in $La_{0.5}Sr_{0.5}FeO_{3-\delta}$ cannot change $\delta=0$ in other air synthesized samples. It is accepted, therefore, that as-synthesized specimens with $x>0$ are fully oxidized also ($\delta=0$).

Different regions can be distinctly seen on the titration isotherm for $La_{0.5}Sr_{0.5}FeO_{3-\delta}$ (Fig. 4). The isotherm behavior in the high-pressure range I reflects the reduction of Fe^{4+} cations:

$$2Fe^{4+} + O^{2-} = 2Fe^{3+} + V_O + \frac{1}{2}O_2 \quad (1)$$

where V_O corresponds to an oxygen vacancy. Then, there is a transition to the range II characterized with a flat shape of the isotherm where oxygen content $(3-\delta)\approx2.75$ is practically independent on oxygen pressure. The predominant defect formation reaction in this region is thermally activated charge disproportionation of Fe^{3+} cations [36].

$$2Fe^{3+} = Fe^{2+} + Fe^{4+} \quad (2)$$

Further depletion of oxygen in the low pressure range III where $(3-\delta)<2.75$ results in reduction of Fe^{3+} cations.

$$2Fe^{3+} + O^{2-} = 2Fe^{2+} + V_O + \frac{1}{2}O_2 \quad (3)$$

Table 2 Thermal expansion coefficients of $La_{0.5}Sr_{0.5}Fe_{1-x}Mn_xO_{3-\delta}$ ceramics

x	Average TECs in air		Average TECs in 5 % CO–5 % CO_2–Ar	
	200–600 °C	800–950 °C	400–600 °C	900–1000 °C
0	12.2±0.8	15.4±1	16±3	20.1±0.2
0.10	11.7±0.7	14.1±0.7	12.4±0.3	16.7±1.5
0.17	11.6±0.8	14.1±0.6	12.4±0.4	18.7±2
0.25	11.5±0.7	13.2±0.5	12.0±0.3	18.2±1.8
0.33	11.3±0.8	13.3±0.3	11.5±0.3	19.2±2

One is observed also in Fig. 4 that substitution of only 10 % of iron with manganese results in disappearance of the plateau on the isotherm in the pressure range II. This behavior can mainly be attributed to reduction of Mn^{4+} cations.

$$2Mn^{4+} + O^{2-} = 2Mn^{3+} + V_O + \frac{1}{2}O_2 \quad (4)$$

Further reduction of Fe^{3+} according to (3) may take place only when all Mn^{4+} and Fe^{4+} cations are exhausted as is evidenced by the coincidence of the coulometric titration curves for x=0 and 0.10 at p_{O_2} <10^{-13} atm in the pressure range III (Fig. 4).

The increase of manganese content results in a number of quantitative changes that reflect competition of defect formation reactions. For instance, the total loss of oxygen is seen to decrease in range I following the decrease in the amount of Fe^{4+} cations available for reaction (1). On the contrary, larger oxygen loss in heavier doped samples can be observed in range II, which suggests manganese cations entering red/ox reaction (4). Generally, one can infer that at relatively high pressures, 10^{-5}<p_{O_2} <0.5 atm, manganese cations in the structure of $La_{0.5}Sr_{0.5}Fe_{1-x}Mn_xO_{3-\delta}$ maintain 4+ oxidation

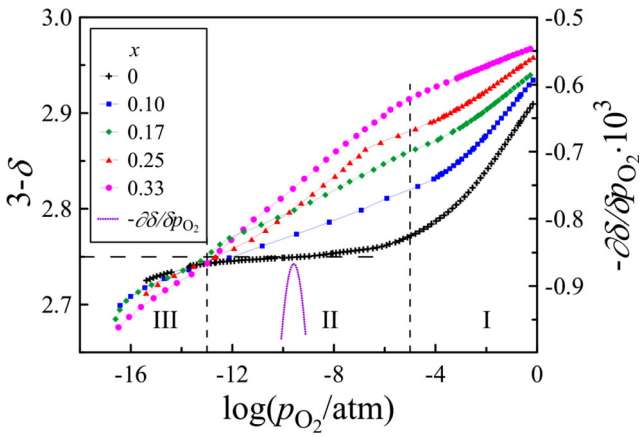

Fig. 4 Isothermal changes of the oxygen content in $La_{0.5}Sr_{0.5}Fe_{1-x}Mn_xO_{3-\delta}$. The maximum of the derivative ($-\partial\delta/\partial p_{O_2}$) corresponds to the equilibrium pressure of oxygen over $La_{0.5}Sr_{0.5}FeO_{2.75}$

degree. The pressure decrease below 10^{-5} atm results in a partial reduction of Mn^{4+} to Mn^{3+} cations. Note also that pressure-induced variations of δ tend to increase with manganese content (Fig. 4). One can expect, therefore, that manganese-rich specimens $La_{0.5}Sr_{0.5}Fe_{1-x}Mn_xO_{3-\delta}$ should have larger thermal expansion at heating in reducing conditions. This conclusion is corroborated by the thermal expansion behavior in reducing atmosphere (Fig. 3b, Table 2). Indeed, one can see that samples with smaller manganese content exhibit larger expansion at T<900 °C, whereas stronger heating, i.e., more harsh reducing environment, results in larger thermal expansion of materials with larger manganese content. The last effect can reflect larger difference in the ionic radii of manganese, Mn^{4+} (R_{CN6}=0.53 Å) vs. Mn^{3+} (R_{CN5}= 0.58 Å), compared to iron cations, Fe^{4+} (R_{CN6}=0.585 Å) vs. Fe^{3+} (R_{CN5}=0.580 Å). Therefore, replacement of iron with manganese may result in increased variations of the average radius of the cations in B sublattice and respectively larger volume changes.

The measured data for electrical conductivity variations with oxygen partial pressure at different temperatures are shown in Fig. 5. The collecting of conductivity data within oxygen pressure limits 10^{-8}–10^{-5} atm involved very lengthy experiments at 950 °C owing to exceedingly sluggish equilibration of the samples. Therefore, the measurements in respective pressure intervals were not performed at lower temperatures. The transitory pressure range is characterized by the change of thermopower sign from positive to negative (Fig. 6). Therefore, the decrease of oxygen pressure over $La_{0.5}Sr_{0.5}Fe_{1-x}Mn_xO_{3-\delta}$ is accompanied by gradual exhaustion of p-type electronic carriers followed by predominance of n-type electronic carriers. Considering large amount of oxygen vacancies in the crystal lattice, one can expect an oxygen ion contribution in addition to n- and p- type components so that the total conductivity of $La_{0.5}Sr_{0.5}Fe_{1-x}Mn_xO_{3-\delta}$ can be represented [37] as

$$\sigma(T, p_{O_2}) = \sigma_i + \sigma_n^0(T)p_{O_2}^{-1/4} + \sigma_p^0(T)p_{O_2}^{+1/4} \quad (5)$$

where σ_i is the ion conductivity, and σ_n^0 and σ_p^0 denote partial contributions from electron- and hole-like carriers

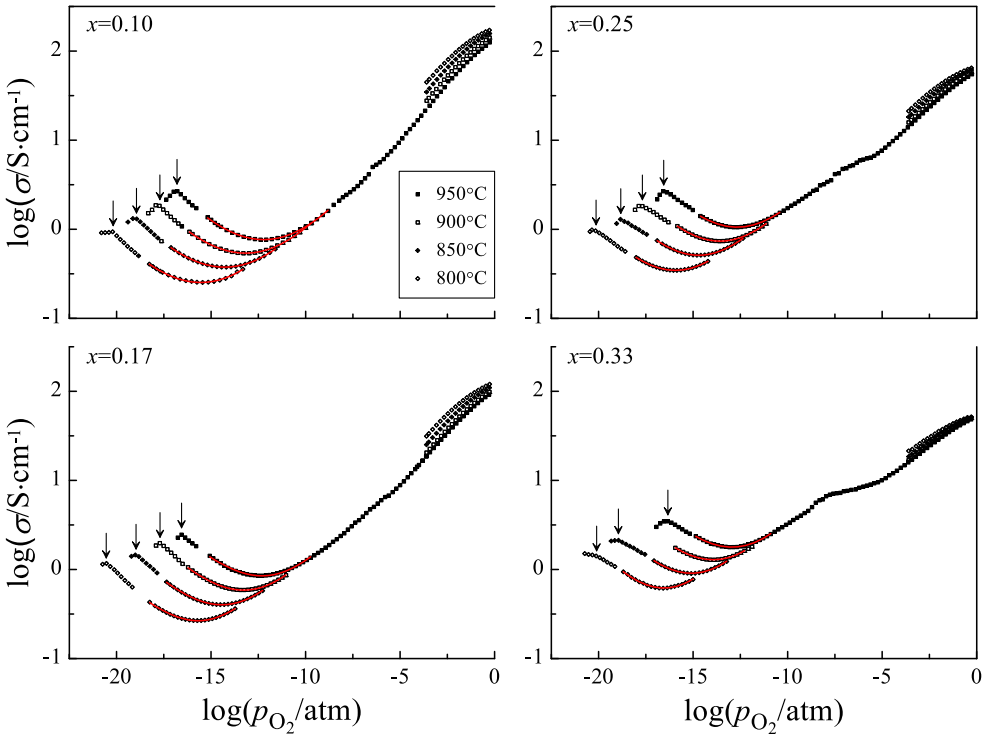

Fig. 5 Electrical conductivity in $La_{0.5}Sr_{0.5}Fe_{1-x}Mn_xO_{3-\delta}$. *Solid lines* show results calculated with the help of Eq. 5. The *arrows* show incipient decomposition

at p_{O_2} =1 atm, respectively. The attempts to describe the experimental data with Eq. (5) where σ_i is a constant result in the calculated ion conductivity values, which increase with manganese content. On the other hand, the oxygen vacancy concentration is seen to decrease with the doping level (Fig. 4), and this change is expected to be accompanied with the decrease of the ion conductivity. From this consideration and taking in view large variations of oxygen vacancy concentration with pressure, one can suppose that the ion contribution in $La_{0.5}Sr_{0.5}Fe_{1-x}Mn_xO_{3-\delta}$ may depend on concentration $(3-\delta)$ of oxygen ions and positions (δ) available for their jumps as

$$\sigma_i(T, p_{O_2}) = \sigma_i^0(T)\delta(3-\delta) \quad (6)$$

where $\sigma_i^0(T)$ is a constant. The approximation of the

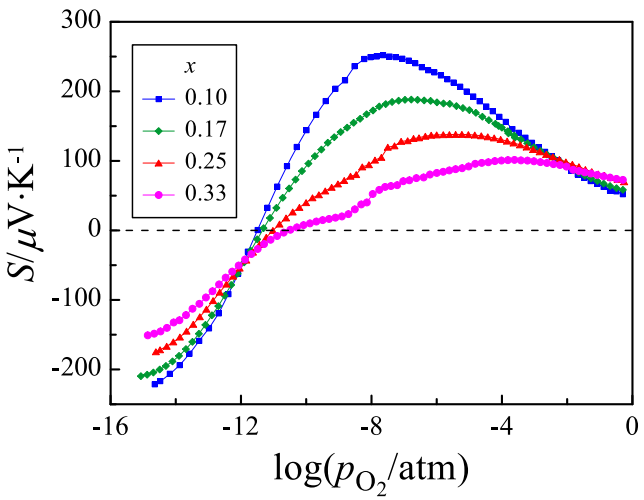

Fig. 6 Isothermal variations of thermopower in $La_{0.5}Sr_{0.5}Fe_{1-x}Mn_xO_{3-\delta}$. *Lines* are guides to the eye

Table 3 The conductivity parameters of $La_{0.5}Sr_{0.5}Fe_{1-x}Mn_xO_{3-\delta}$

x	T, °C	σ_i^0/S·cm^{-1}	σ_n^0/S·cm^{-1}·atm$^{1/4}$	σ_p^0/S·cm^{-1}·atm$^{-1/4}$
	950	0.643±0.006	(1.31±0.01)×10^{-4}	194±2
	900	0.462±0.002	(5.18±0.03)×10^{-5}	233±1
0.10	850	0.323±0.001	(1.926±0.008)×10^{-5}	304±1
	800	0.212±0.003	(6.5±0.1)×10^{-6}	435±8
	950	0.73±0.01	(1.36±0.03)×10^{-4}	254±4
	900	0.485±0.007	(5.75±0.07)×10^{-5}	319±4
0.17	850	0.329±0.004	(2.08±0.02)×10^{-5}	427±4
	800	0.213±0.003	(6.95±0.09)×10^{-6}	593±7
	950	0.80±0.01	(1.60±0.02)×10^{-4}	403±4
	900	0.542±0.05	(6.90±0.06)×10^{-5}	483±3
0.25	850	0.362±0.001	(2.621±0.008)×10^{-5}	667±2
	800	0.252±0.003	(8.56±0.09)×10^{-6}	889±9
	950	1.22±0.05	(2.37±0.04)×10^{-4}	898±8
	900	0.868±0.008	(9.94±0.08)×10^{-5}	1165±7
0.33	850	0.551±0.007	(4.02±0.04)×10^{-5}	1697±12
	800	0.33±0.01	(1.34±0.03)×10^{-5}	2847±51

experimental isotherms with the help of Eq. (5) is shown with solid lines in Fig. 5. The fitted values for σ_i^0, σ_n^0, and σ_p^0 at different temperatures are collected in Table 3. The oxygen vacancies are considered as random and equally available for the transport process, while possible effects of local ordering are neglected in Eq.(6). This supposition appears to be viable because oxygen vacancies in the parent $La_{01-x}Sr_xFeO_{3-\delta}$ seem to be mostly randomized at $0<x\leq 0.5$ [16].

The data in Table 3 can be used in order to draw Arrhenius plots for ion and *n*-type contributions to the total conductivity (Fig. 7). The respective apparent activation energies, E_i and E_n, are shown in Table 4. The obtained E_i values are in the range of 0.7–1.1 eV, which is quite typical for oxygen ion conductors [38] and additionally speaks in favor of the used model. Note also that E_i's tend to increase with manganese content. This behavior is consistent with the doping-induced compression of the crystalline lattice that hinders diffusion jumps of large oxygen ions (Table 1).

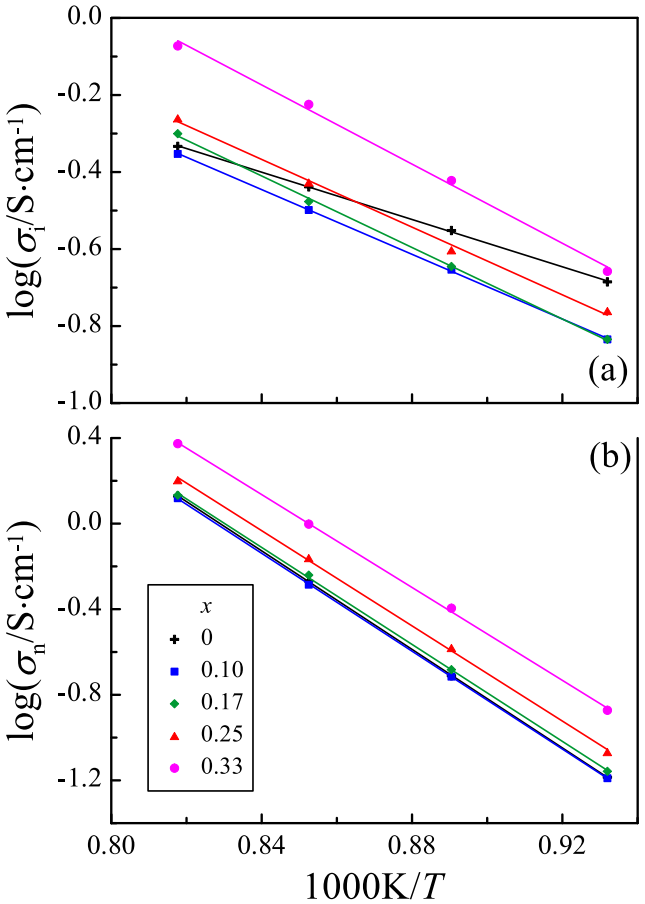

Fig. 7 Arrhenius plots for ion conductivity in $La_{0.5}Sr_{0.5}Fe_{1-x}Mn_xO_{3-\delta}$ at δ=0.25 (**a**) and electron *n*-type conductivity at p_{O_2} =10^{-16} atm (**b**). Data for x=0 are taken from [16]

Table 4 The apparent activation energy values for ion and electron conductivity in $La_{0.5}Sr_{0.5}Fe_{1-x}Mn_xO_{3-\delta}$ at δ=0.25 and p_{O_2} = 10^{-16} atm, respectively

x	E_i, eV	E_n, eV
0	0.71±0.01	2.38±0.01
0.10	0.93±0.01	2.36±0.01
0.17	1.02±0.02	2.34±0.03
0.25	0.97±0.03	2.30±0.04
0.33	1.12±0.04	2.25±0.03

The overall increase in the ion conductivity values with manganese content in $La_{0.5}Sr_{0.5}Fe_{1-x}Mn_xO_{3-\delta}$ may be understood taking in view preference of Fe^{3+} and Mn^{3+} cations to tetrahedral and fivefold oxygen coordination, respectively [39, 24, 25]. While a tetrahedrally coordinated Fe^{3+} cation serves as a trap for two oxygen vacancies, its replacement for a fivefold coordinated Mn^{3+} cation results in release of one vacancy to be involved in the ion transport. In the result, the ion conductivity tends to increase with doping. The effect becomes noticeable when percolation threshold is achieved at x=0.25, and at x=0.33, ion conductivity attains almost twice larger values than in the parent ferrite $La_{0.5}Sr_{0.5}FeO_{3-\delta}$.

The activation energy for *n*-type contribution 2.3–2.4 eV occurs virtually independent on manganese content thus demonstrating electron transport mediated mostly by Fe^{2+} cations. The observed increase of electron conductivity level (Fig. 7b), with manganese content can be interrelated with respective decrease in amount of iron-oxygen tetrahedra FeO_4 that are known to hamper electron transport [40].

The comparison of the hole conductivity in oxidizing and reducing conditions is seen in Fig. 8. The experimental values at p_{O_2} =0.21 atm are shown in Fig. 8a. Similar data were calculated also at p_{O_2} =10^{-8} atm from $\sigma_p\left(T,p_{O_2}\right)=\sigma_p^0(T)$ $p_{O_2}^{+1/4}$ with the using of the results in Table 3 and Fig. 8b. The hole conductivity in air conditions is seen to decrease with the increase of manganese content, which reflects replacement of Fe^{4+} by Mn^{4+} cations that do not take part in transport of electron holes. One can note also from comparison of the data at 950 °C in Figs. 2 and 8a that oxygen loss is not quite proportional to conductivity decrease with the increase of manganese content. Therefore, replacement of manganese for iron results in decrease of both concentration and mobility of *p*-type carriers, which again is consistent with exclusion of Mn^{4+} cations from hole transport at high pressures of oxygen. Quite different is the behavior of the hole contribution in $La_{0.5}Sr_{0.5}Fe_{1-x}Mn_xO_{3-\delta}$ at low pressures of oxygen (Fig. 8b). It is seen that the increase of manganese content from 0 to 0.33 is accompanied with almost fivefold increase of the *p*-type conductivity. Considering strong exhaustion of Fe^{4+} and equilibration of Mn^{3+} and

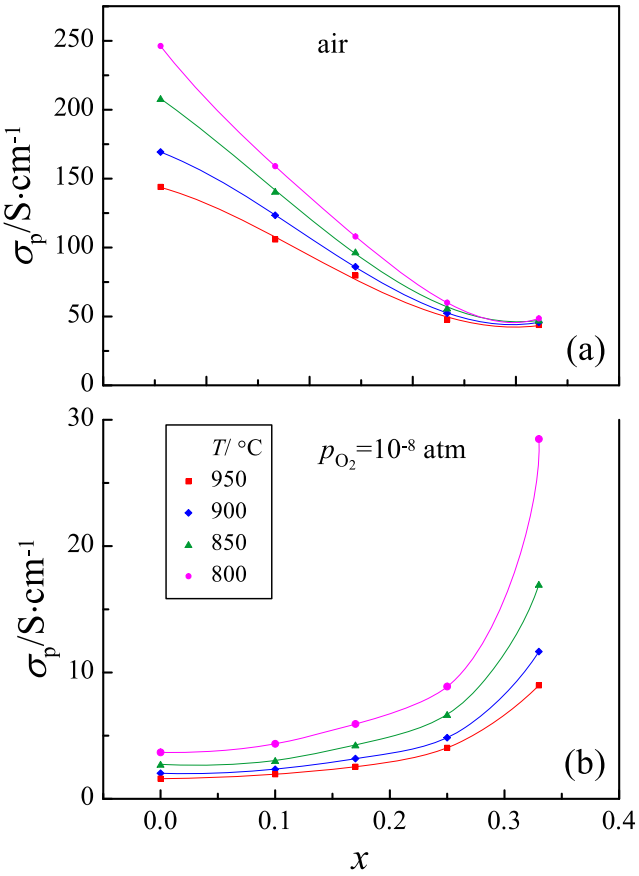

Fig. 8 The *p*-type contribution to the total conductivity in $La_{0.5}Sr_{0.5}Fe_{1-x}Mn_xO_{3-\delta}$ at p_{O_2} =0.21 (**a**) and p_{O_2} =10^{-16} atm (**b**). *Lines* are guides to the eye. Data for x=0 are taken from [16]

Mn^{4+} cations at 10^{-8} atm, this change may be interpreted as an indication of manganese cations being involved in the electron transport.

It is noted above that a sharp decline of conductivity is signaling the incipient decomposition of the oxides at low pressures of oxygen. Therefore, the positions of the cusps on the isotherms in Fig. 5 can be used in order to draw respective temperature-dependent plots for oxygen pressure $p_{O_2}^{red}$ of reductive decomposition at different manganese content in $La_{0.5}Sr_{0.5}Fe_{1-x}Mn_xO_{3-\delta}$ (Fig. 9). Similar data for $LaFeO_3$ and $LaMnO_3$ [10] show that the stability of the doped derivatives at reduction is falling in between stability of $LaFeO_3$ and $LaMnO_3$.

The ion conductivity at 950 °C and different pressures of oxygen is shown in Fig. 10. While oxygen ion conductivity in $La_{0.5}Sr_{0.5}FeO_{3-\delta}$ is seen to weakly change in a wide pressure range as suggested earlier [16], it is not so in manganese-doped derivatives where considerable variations of oxygen non-stoichiometry persist near intrinsic electron–hole equilibrium. In order to evaluate the capability of $La_{0.5}Sr_{0.5}Fe_{1-x}Mn_xO_{3-\delta}$ as

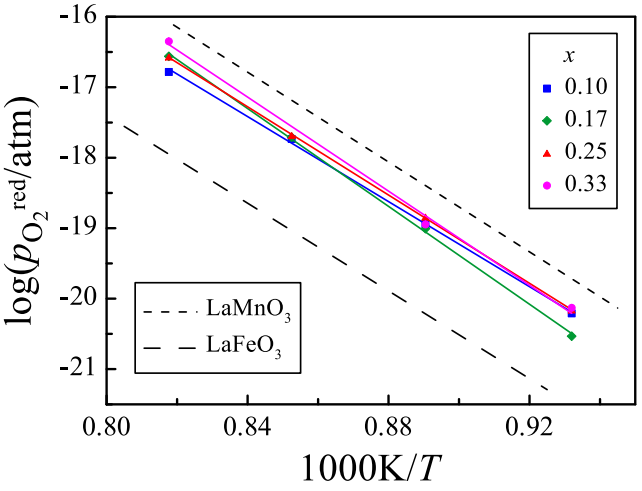

Fig. 9 Decomposition pressure limits $p_{O_2}^{red}$ for $La_{0.5}Sr_{0.5}Fe_{1-x}Mn_xO_{3-\delta}$ at different manganese content. Data for $LaFeO_{3-\delta}$ and $LaMnO_{3-\delta}$ are taken from [10]

oxygen separating membrane material, one can use the Wagner equation for oxygen permeate flux density [41]

$$j(O_2) = \frac{RT}{16F^2L}\int_{p''}^{p'} \frac{\sigma_i\cdot(\sigma_n+\sigma_p)}{\sigma_i+\sigma_n+\sigma_p} d\ \ln\ p_{O_2} \qquad (7)$$

where F is the Faraday constant, L is the thickness of the membrane, R is the gas constant, p' and p'' are oxygen pressure values at the high- and low-pressure sides of the membrane, respectively. The accordingly calculated results for the membranes with the thickness of 0.1 cm at 950 °C are exhibited in Fig. 11. The plots show changes of the oxygen permeate flux density with pressure variations at the low-pressure side, while the

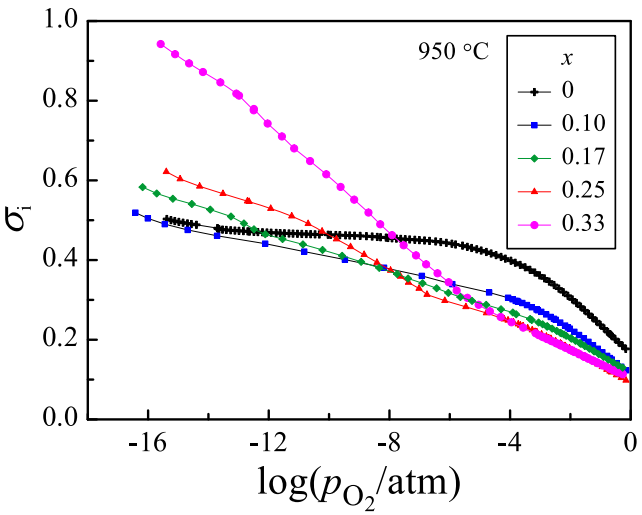

Fig. 10 The ion conductivity $\sigma_i=\sigma_i^0\cdot\delta\cdot(3-\delta)$ in $La_{0.5}Sr_{0.5}Fe_{1-x}Mn_xO_{3-\delta}$ vs. oxygen partial pressure

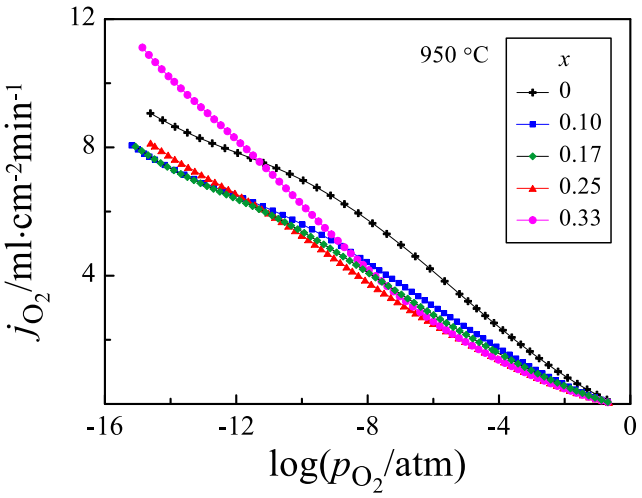

Fig. 11 The calculated oxygen permeation fluxes for $La_{0.5}Sr_{0.5}Fe_{1-x}Mn_xO_{3-\delta}$ ceramic membranes at different values of oxygen partial pressure at the permeate side. The feed side is flushed by air. The Wagner Eq. 7 was used for calculations. The membrane thickness is 0.1 cm. The temperature is 950 °C. Data for x=0 are taken from [16]

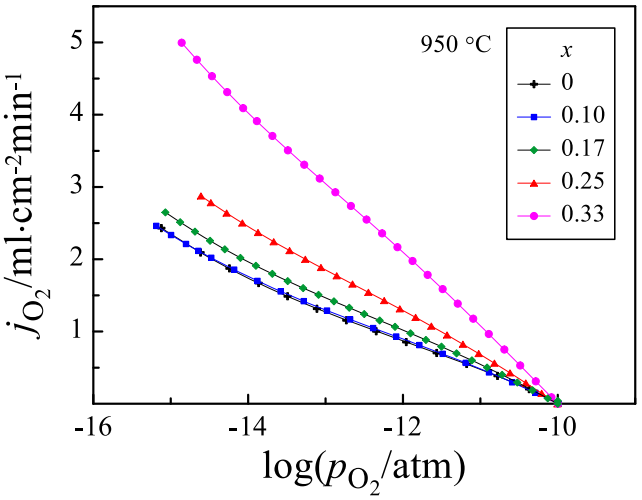

Fig. 12 The calculated oxygen flux density for $La_{0.5}Sr_{0.5}Fe_{1-x}Mn_xO_{3-\delta}$ ceramic membranes at different values of oxygen partial pressure at the permeate side. The feed side is flushed by steam. The oxygen pressure 10^{-10} atm in flowing steam is maintained due to hydrogen formed in the water splitting process (~0.3 % H_2). The membrane thickness is 0.1 cm. The temperature is 950 °C. Data for x=0 are taken from [16]

high-pressure side is flushed by air (p_{O_2} =0.21 atm). The substitution of iron by manganese results in smaller flux values compared to the parent ferrite when relatively small pressure gradients are applied to the membrane. This finding is consistent with the literature data. For instance, authors [26] observed that oxygen permeation rate of $SrFe_{1-x}Mn_xO_{3-\delta}$ at 900 °C tends to decrease with the increase of manganese content in experiments under He/air gradient. Similar conclusion is drawn in work [27] where oxygen diffusion was studied in $La_{1-x}Sr_xFe_{1-y}Mn_yO_{3-\delta}$ by means of TG relaxations as results of atmosphere change from N_2 to 50 %N_2–50 %O_2. However, the tendency can be seen for the separating efficiency to increase with manganese doping and oxygen pressure gradient so that the oxygen flux through the oxide with x=0.33 attains about 20 % higher values compared to x=0 at 10^{-15} atm/0.21 atm oxygen pressure difference applied to the membrane. One can see from Fig. 10 that oxygen flux is rather heavily hampered due to relatively low oxygen ion conductivity of $La_{0.5}Sr_{0.5}Fe_{1-x}Mn_xO_{3-\delta}$ in oxidative conditions. Therefore, larger oxygen permeability of $La_{0.5}Sr_{0.5}Fe_{1-x}Mn_xO_{3-\delta}$ in comparison with $La_{0.5}Sr_{0.5}FeO_{3-\delta}$ can be expected when the high-pressure side of the membrane is flushed by oxygen containing gaseous phase with oxygen pressure (activity) lower than in the air. For instance, when steam is used in place of air, the oxygen permeability of $La_{0.5}Sr_{0.5}Fe_{0.67}Mn_{0.33}O_{3-\delta}$ is seen to be about 100 % larger compared to $La_{0.5}Sr_{0.5}FeO_{3-\delta}$ (Fig. 12). This mode of the membrane operation can be used in order to obtain pure hydrogen from water vapor in addition to syngas at the side flushed by methane. Certainly, the calculations with Eq. 7 provide only an upper possible limit of the flux because surface oxygen exchange reactions can hinder the overall ion transport and result in somewhat smaller flux values. Still, the estimates seem to be rather satisfactory because calculated and experimental flux values for ferrous membranes coincide fairly well at elevated temperatures [17] thus showing quite fast surface kinetics.

Conclusion

Manganese-doped derivatives of perovskite-like $La_{0.5}Sr_{0.5}FeO_{3-\delta}$, one of most promising ferrite materials for high-temperature electrochemical applications, were synthesized via solid-state synthesis route. The parameters of the rhombohedral unit cell (S.G. $R\bar{3}c$) in $La_{0.5}Sr_{0.5}Fe_{1-x}Mn_xO_{3-\delta}$ were found to decrease on doping, which reflects replacement of iron with smaller manganese cations. The oxygen losses and dimensional changes at heating in oxidizing conditions (air) both decrease with increasing manganese content. At the same time, thermal expansion under reducing conditions was observed to increase with manganese content.

The conductivity measurements reveal several regions of the oxygen partial pressure with different doping-dependent behavior. The high-pressure range (p_{O_2} >10^{-5} atm) is characterized by the total conductivity level lower in the substituted perovskites compared to the parent phase. This occurs as Fe^{4+} cations associated with mobile holes are replaced by Mn^{4+} that do not take part in the p-type electron transport. Quite different conductivity behavior is observed in the low-

pressure limit (p_{O_2} $<10^{-8}$ atm) where all three contributions, i.e. oxygen ion, *p*- and *n*-type components, increase with manganese content.

The estimates based on the Wagner equation show that oxygen permeability of $La_{0.5}Sr_{0.5}Fe_{0.67}Mn_{0.33}O_{3-\delta}$ at 950 °C may attain about 20 % higher values compared to $La_{0.5}Sr_{0.5}FeO_{3-\delta}$ when oxygen pressure gradient across the membrane is large enough. Even higher oxygen permeability can be achieved when steam is used in place of air. In combination with a satisfactory stability in reducing environments, these findings suggest that $La_{0.5}Sr_{0.5}Fe_{0.67}Mn_{0.33}O_{3-\delta}$ can be considered as a promising membrane material in integrated reactors for oxygen separation, hydrogen production, and partial oxidation of hydrocarbons.

Acknowledgments The authors are grateful to the Government of the Sverdlovsk Region and the Russian Foundation for Basic Research (Contracts No. 13-08-96060-Ural, No.13-03-00931), and the Russian Academy of Sciences (Contract No.15-15-3-27-Arctica) for the partial support of this work.

References

1. Bouwmeester HJM (2003) Catal Today 82:141–150
2. Geffroy P-M, Fouletier J, Richet N, Chartier T (2013) Chem Eng Sci 87:408–433
3. Wei Y, Yang W, Caro J, Wang H (2013) Chem Eng J 220:185–203
4. Sunarso J, Baumann S, Serra JM, Meulenberg WA, Liu S, Lin YS, da Costa JCD (2008) J Membr Sci 320:13–41
5. Dong XL, Jin WQ, Xu NP, Li K (2011) Chem Commun 47:10886–10902
6. Dyer PN, Richards RE, Russek SL, Taylor DM (2000) Solid State Ionics 134:21–33
7. Teraoka Y, Zhang HM, Furukawa S, Yamazoe N (1985) Chem Lett 14:1743–1746
8. Wang H, Tablet C, Feldhoff A, Caro J (2005) J Membr Sci 262:20–26
9. Lein HL, Wiik K, Grande T (2006) Solid State Ionics 177:1795–1798
10. Nakamura T, Petzow G, Gauckler LJ (1979) Mater Res Bull 14:649–659
11. Feldhoff A, Martynczuk J, Wang H (2007) Prog Solid State Chem 35:339–353
12. Martynczuk J, Liang F, Arnold M, Šepelák V, Feldhoff A (2009) Chem Mater 21:1586–1594
13. Tian T, Wang W, Zhan M, Chen C (2010) Catal Commun 11:624–628
14. Wang Y, Liao Q, Zhou L, Wang H (2014) J Membr Sci 457:82–87
15. Kozhevnikov VL, Leonidov IA, Patrakeev MV, Markov AA, Blinovskov YN (2009) J Solid State Electrochem 13:391–395
16. Patrakeev MV, Bahteeva JA, Mitberg EB, Leonidov IA, Kozhevnikov VL, Poeppelmeier KR (2003) J Solid State Chem 172:219–231
17. Markov AA, Patrakeev MV, Leonidov IA, Kozhevnikov VL (2011) J Solid State Electrochem 15:253–257
18. Patrakeev MV, Markov AA, Leonidov IA, Kozhevnikov VL, Kharton VV (2006) Solid State Ionics 177:1757–1760
19. Waerenborgh JC, Rojas DP, Shaula AL, Mather GC, Patrakeev MV, Kharton VV, Frade JR (2005) Mater Lett 59:1644–1648
20. Markov AA, Patrakeev MV, Savinskaya OA, Nemudry AP, Leonidov IA, Leonidova ON, Kozhevnikov VL (2008) Solid State Ionics 179:99–103
21. Mizusaki J (1992) Solid State Ionics 52:79–91
22. Kozhevnikov VL, Leonidov IA, Bahteeva JA, Patrakeev MV, Mitberg EB, Poeppelmeier KR (2004) Chem Mater 16:5014–5020
23. Poeppelmeier KR, Leonowicz ME, Scanlon JC, Longo JM, Yelon WB (1982) J Solid State Chem 45:71–79
24. Suescun L, Chmaissem O, Mais J, Dabrowski B, Jorgensen JD (2007) J Solid State Chem 180:1698–1707
25. Shaula AL, Markov AA, Naumovich EN, Waerenborgh JC, Pivak YV, Kharton VV (2012) Solid State Ionics 225:206–210
26. Kato S, Kikawa D, Ogasawara M, Moriya Y, Sugai M, Nakata S (2005) Solid State Ionics 176:1377–1381
27. Mikkelsen L, Andersen IGK, Skou EM (2002) Solid State Ionics 152–153:703–707
28. Mizusaki J, Mori N, Takai H, Yonemura Y, Minamiue H, Tagawa H, Dokiya M, Inaba H, Naraya K, Sasamoto T, Hashimoto T (2000) Solid State Ionics 129:163–177
29. Rodríguez-Carvajal J (1993) Physica B 192:55–69
30. Patrakeev MV, Leonidov IA, Kozhevnikov VL (2011) J Solid State Electrochem 15:931–954
31. Goldyreva EI, Leonidov IA, Patrakeev MV, Chukin AV, Leonidov II, Kozhevnikov VL (2015) J Alloys Compd 638:44–49
32. Patrakeev MV, Leonidov IA, Kozhevnikov VL, Poeppelmeier KR (2005) J Solid State Chem 178:921–927
33. Dann SE, Currie DB, Weller MT, Thomas MF, Al-Rawwas AD (1994) J Solid State Chem 109:134–144
34. Shannon RD (1976) Acta Crystallogr Sect A 32:751–767
35. Park CY, Jacobson AJ (2005) J Electrochem Soc 152:J65–J73
36. Mizusaki J, Ychihiro M, Yamauchi S, Fueki K (1985) J Solid State Chem 58:257–266
37. Kröger FA (1964) The chemistry of imperfect crystals. North Holland Publishing Co, Amsterdam
38. Kharton VV, Marques FMB, Atkinson A (2004) Solid State Ionics 174:135–149
39. Starkov I, Bychkov S, Matvienko A, Nemudry A (2014) Phys Chem Chem Phys 16:5527–5535
40. Patrakeev MV, Kharton VV, Bakhteeva YA, Shaula AL, Leonidov IA, Kozhevnikov VL, Naumovich EN, Yaremchenko AA, Marques FMB (2006) Solid State Sci 8:476–487
41. Bouwmeester JM, Burgraaf AJ (1996) Dense ceramic membranes for oxygen seperation. In: Burgraaf AJ, Cot L (eds) Fundamentals of inorganic membrane science and technology. Elsevier, Amsterdam, p 435